

## **Cytochrome P450 Architecture and Cysteine Nucleophile Placement Impacts Raloxifene Mediated Mechanism-Based Inactivation.**

Brooke M. VandenBrink, John A. Davis, Josh T. Pearson, Robert S. Foti, Larry C. Wienkers and Dan A. Rock

Biochemistry and Biophysics Group, Departments of Pharmacokinetics and Drug Metabolism, Amgen Inc, 1201 Amgen Court West, Seattle, WA 98119-3105 (BMV, JAD, JTP, RSF, LCW and DAR)

## Running Title Page

Running Title: Raloxifene Selective CYP Inactivation

Address for Correspondence:

Dan A Rock

1201 Amgen Court West

Seattle, WA 98119.

Ph: (206) 265-7139.

Fax: (206) 265-1149

E-mail: [drock@amgen.com](mailto:drock@amgen.com).

Text pages: 26

Tables: 2

Figures: 5

References: 48

Abstract words: 241

Introduction words: 775

Discussion words: 1,504

Abbreviations: TDI, time dependent inhibition; CYP, cytochrome P450; HLM, human liver microsomes; MBI, mechanism-based inactivation; LC-MS/MS, liquid chromatography-tandem mass spectrometry; ACN, acetonitrile

## Abstract

The propensity for cytochrome P450 (CYP) enzymes to bioactivate xenobiotics is governed by the inherent chemistry of the xenobiotic itself and the active site architecture of the P450 enzyme(s). Accessible nucleophiles in the active site or egress channels of the P450 enzyme have the potential of sequestering reactive metabolites through covalent modification, thereby limiting their exposure to other proteins. Raloxifene, a drug known to undergo CYP3A-mediated reactive metabolite formation and time-dependent inhibition *in vitro*, was utilized to explore the potential for bioactivation and enzyme inactivation of additional CYP enzymes (CYP1A2, CYP2C8, CYP2C9, CYP2C19, CYP2D6, CYP2E1 and CYP3A5). Every CYP tested except CYP2E1 was capable of raloxifene bioactivation, based on glutathione adduct formation. However, raloxifene mediated time-dependent inhibition only occurred in CYP2C8 and CYP3A4. Comparable inactivation kinetics were achieved with a  $K_i$  and  $k_{inact}$  values of 0.26  $\mu\text{M}$  and 0.10  $\text{min}^{-1}$ , 0.81  $\mu\text{M}$  and 0.20  $\text{min}^{-1}$  for CYP2C8 and CYP3A4, respectively. Proteolytic digests of CYP2C8 and CYP3A4 Supersomes<sup>TM</sup> revealed adducts to Cys225 and Cys239 for CYP2C8 and CYP3A4, respectively. For each CYP enzyme, proposed substrate/metabolite access channels were mapped and active site cysteines were identified, which revealed only CYP2C8 and CYP3A4 possess accessible cysteine residues near the active site cavities, a result consistent with the observed kinetics. The combined data suggest the extent of bioactivation across CYP enzymes does not correlate to CYP inactivation. In addition, multiple factors contribute to the ability of reactive metabolites to form apo-adducts with a CYP enzyme.

## Introduction

The cytochrome CYP enzyme (CYP) family is largely responsible for the metabolism of xenobiotics (Guengerich, 2001; Wienkers and Heath, 2005). Although CYP-mediated metabolism usually leads to detoxification, bioactivation and reactive metabolites formation can occur increasing the risk of drug-induced liver injuries (Mitchell et al., 1973; Dahlin et al., 1984; Leung et al., 2012). A key differentiating factor for a xenobiotic to form a benign, oxidative metabolite or a reactive metabolite is the innate chemistry of the xenobiotic (Nelson, 1982). The term structural alert classifies a set of chemical functional groups prone to CYP-mediated reactive metabolite formation (Kalgutkar and Didiuk, 2009; Stepan et al., 2011). Exposure of these functional groups to CYP enzymes is anticipated to increase the probability of reactive metabolite formation; therefore, strategies to identify and limit reactive metabolite formation are of importance.

Substrate interactions with the active site architecture of CYP enzymes also governs regioselectivity of metabolite formation, potentially impacting bioactivation and exposure to reactive metabolites. For example, furafylline possesses a structural alert in the furan moiety. However, bioactivation has been shown to occur exclusively at the 8-methyl position of the xanthine moiety (Kunze and Trager, 1993). Docking studies with furafylline and CYP1A2 position the 8-methyl position towards the heme iron based upon a prominent interaction between the furan ring and Phe125 of the enzyme active site, highlighting the potential for enzyme to direct metabolite regioselectivity (Lewis and Lake, 1996). CYP active site architecture not only orients substrate potentially limiting formation of reactive metabolites, but can also sequester bioactivated metabolites through covalent trapping by accessible nucleophiles. Reactive metabolites trapped in the active site by nucleophilic amino acids directly limits tissue exposure; thereby, decreasing the release of reactive metabolites and indirectly, the potential toxicity of bioactivation via feedback inhibition (Pearson et al., 2007).

Over the last decade, the X-ray crystal structures of CYPs offered structural insights to the active site topography and defined key residue interactions with co-crystallized ligands (Johnson and Stout, 2005; Dong and Wu, 2012). This structural information facilitates the location of nucleophilic residues within the active site of CYP enzymes. A substrate prone to reactive metabolite formation could be used to probe the location of relevant active site nucleophiles. CYP-mediated reactive metabolite formation and subsequent enzyme inactivation typically have one of three fates: the reactive metabolite adducts the heme, forms a metabolic-intermediate complex with the heme or covalently adducts the apo-protein (Kalgutkar et al., 2007). Alkynes and alkyl amine containing compounds are classic examples where the reactive metabolites react with the heme and heme iron, respectively (Chan et al., 1993; Hanson et al., 2010). In this instance, the reactive metabolite formed has relatively the same potential for reactivity across CYP enzymes given the conserved nature of the heme. However, some reactive metabolites are preferentially quenched by nucleophilic amino acid residues in the active site, which leads to CYP inactivation (Baer et al., 2007; Henne et al., 2012; Lin et al., 2012). The structure of reactive metabolites is commonly inferred by identification of glutathione adducts (Baillie et al., 1989; Dieckhaus et al., 2005). The cysteine thiol in glutathione represents a delocalized (soft) electrophile with vast reactivity and is physiologically relevant given the high cellular concentrations. As such, glutathione-adducted xenobiotics are commonly inferred to be the chemical entities responsible for CYP inactivation through apo-adduct formation.

Raloxifene undergoes bioactivation and formation of glutathione adducts *in vitro* by both CYP3A4 and CYP3A5. However, raloxifene is a time-dependent inhibitor of only CYP3A4 (Pearson et al., 2007). The difference in inhibition was attributed to a single cysteine residue (Cys239) that is present in CYP3A4 but not CYP3A5. Cys239 sits at the interface between the active site and bulk solvent. Blocking this residue with iodoacetamide and/or mutating the cysteine to alanine, led to an increase in the formation of reactive metabolites from raloxifene as inferred from the increase in glutathione-conjugated raloxifene. The increase in glutathione-

adducted raloxifene was even more dramatic in CYP3A5. Although the raloxifene adduct findings are not physiologically relevant due to limited role of CYP metabolism in the in vivo clearance (Kemp et al., 2002), other xenobiotics including AMG 478 (Henne et al., 2012) and carbamazepine (Kang et al., 2008) have been shown to or proposed to form adducts with Cys239.

The work presented herein investigates the potential role of active site cysteine residues across a panel of CYP enzymes for their ability to trap reactive metabolites. Raloxifene was used as a probe to explore the potential for bioactivation and inactivation across eight CYPs (CYP 1A2, 2C8, 2C9, 2C19, 2D6, 2E1, 3A4 and 3A5). In addition, the amino acid architecture of the CYP active sites were examined and discussed in terms of the observed kinetic data.

## Materials and Methods

**Materials.** Supersomes™ co-expressed with cytochrome b<sub>5</sub> and P450 reductase were purchased from BD Biosciences (Woburn, MA). Trypsin and proteinase K were purchased from Roche Diagnostics (Indianapolis, IN). Raloxifene, tolbutamide, diclofenac, dextromethorphan, dextrorphan, midazolam, 1'-hydroxymidazolam, 6β-hydroxytestosterone, paclitaxel, reduced glutathione and chlorzoxazone were purchased from Sigma Chemical Co. (St. Louis, MO). (S)-mephenytoin was purchased from Biomol International (Plymouth Meeting, PA). 6-Hydroxypaclitaxel and reduced β-NADPH were purchased from Calbiochem (San Diego, CA). 4'-Hydroxy-(S)-mephenytoin, 4'-hydroxydiclofenac, 6-hydroxychlorzoxazone were purchased from BD Biosciences (Bedford, MA). Phenacetin and acetaminophen were purchased from MP Biomedicals (Solon, OH). Testosterone was purchased from Steraloids (Newport, RI). All other chemicals and liquid chromatography solvents were acquired from commercial sources, and were of the highest grade available.

*Measurement of raloxifene IC<sub>50</sub> values, IC<sub>50</sub> shift assays and time-dependent inhibition.* IC<sub>50</sub> values of raloxifene were determined against both testosterone and midazolam. Prior to conducting IC<sub>50</sub> measurements,  $K_m$  and  $k_{cat}$  values for both testosterone and midazolam were determined for each enzyme studied (data not shown) and the results were consistent with published data (Dickmann et al., 2012). Varying concentrations of raloxifene (0-100 μM) were pre-incubated with enzyme (1 picomole per 100 μL final incubation volume) and substrate (at the pre-determined  $K_m$  value) for 5 min before initiation of the reaction with NADPH. The reactions were quenched after 5 min for midazolam or 20 min for testosterone with an equal volume (100 μL) of 0.5 μM tolbutamide in acetonitrile. Incubations were run in triplicate and IC<sub>50</sub> values determined in Prism 5.0 (GraphPad Software, San Diego California USA, [www.graphpad.com](http://www.graphpad.com)). The IC<sub>50</sub> values were used to demonstrate the potential for raloxifene to reversibly bind to the eight CYPs under investigation and provide an appropriate initial estimate

for raloxifene concentrations in the subsequent TDI experiments.  $IC_{50}$  shift experiments were set under similar conditions and as previously reported (Henne et al., 2012). For raloxifene  $IC_{50}$  and time-dependent inhibition studies, a 4000Q-Trap from Applied Biosystems (San Jose, CA) was used and interfaced to a Shimadzu HPLC. MS parameters for each metabolite measured are listed in Supplemental Table 1. Common to all compounds was the dwell time, 500 ms; curtain gas, 10; IonSpray voltage, 4500; source temperature, 400 °C; IonSpray gas 1 and 2 were set at 40.

*Raloxifene metabolism and glutathione adduct formation.* Individual CYP enzymes (10 pmol) were pre-incubated for 5 min at 37 °C prior to the addition of 10 mM NADPH to a final concentration of 1 mM (1 mL total volume) in the presence of 10  $\mu$ M raloxifene and 1 mM glutathione (GSH). Aliquots were removed from the incubation at 0, 3, 6, 9, 12 and 15 min and placed into 100  $\mu$ L of cold acetonitrile spiked with 0.5  $\mu$ M tolbutamide for an internal standard. All incubations were run in triplicate. Remaining concentrations of raloxifene were measured using 4000 Q-Trap using MRM scan with the Q1  $m/z$  474.3 and the Q3  $m/z$  111.9. The declustering potential was 66 and collision energy of 47. Tolbutamide was monitored by a Q1  $m/z$  271.2 and the Q3  $m/z$  91.1. Common to both compounds was the dwell time, 500ms, curtain gas, 10; IonSpray voltage, 4500; source temperature, 400 °C; IonSpray gas 1 and 2 were set at 40. Time-dependent inhibition was characterized for CYP3A4 and CYP2C8 based on the  $IC_{50}$  shift results. The assay was performed with a two-step procedure in a 96-well format. Each time point was sampled in triplicate. Inactivation in preincubation mixtures was conducted in potassium phosphate buffer (100 mM, pH 7.4) containing CYP3A4 or CYP2C8 Supersomes™ and raloxifene (0-10  $\mu$ M). After a 3 min equilibration at 37°C, reactions were initiated by addition of NADPH (1 mM) in a final incubation volume of 0.2 mL. Reactions proceeded for 0, 2, 4, 6, or 10 min at which time aliquots (10  $\mu$ L) were transferred to an activity assay for assessment of remaining CYP activity. Incubations (pre-warmed to 37°C) contained

NADPH (1 mM) and either midazolam for CYP3A4 (10  $\mu$ M) or paclitaxel for CYP2C8 (200  $\mu$ M) in potassium phosphate buffer (100 mM, pH 7.4). The final volume was 0.2 mL. Reactions were allowed to precede 5 min and were terminated by addition of an equal volume of ACN containing tolbutamide (0.5  $\mu$ M) as an internal standard. Quenched mixtures were vortex mixed and centrifuged and resulting supernatants were analyzed via LC-MS/MS as described above. Kinetic parameters were determined using GraphPad Prism (GraphPad Software Inc., La Jolla, CA). The natural log of percent remaining CYP3A4 activity versus pre-incubation time was plotted for each inhibitor concentration, and initial inactivation rate constants ( $k_{obs}$ ) were calculated from the linear portions of the slopes of the log-linear portion of each plot. Inactivation parameters were estimated by non-linear regression using the following relationship:  $k_{obs} = [(k_{inact} \times I) / (K_i + I)]$ , where  $K_i$  is the inhibitor concentration at which the rate of enzyme inactivation is half the maximal rate,  $k_{inact}$  is the rate constant for the maximal inactivation rate, and  $I$  is the initial inhibitor concentration (Silverman, 1988).

*CYP Protein and Peptide Adduct Characterization.* CYP2C8 and CYP3A4 Supersomes™ were used to characterize protein adduct formation based upon the TDI data above at (0.4  $\mu$ M) and raloxifene (50  $\mu$ M) were incubated in 0.5 mL potassium phosphate buffer (100 mM, pH 7.4) for 20 min at 37°C in the presence or absence of NADPH. Incubations were subsequently placed on ice and concentrated to a 15  $\mu$ L volume using a Savant SpeedVac (Thermo Scientific, San Jose, CA). Aliquots (400  $\mu$ L) of ammonium bicarbonate buffer (50 mM, pH 8.1) and methanol (50  $\mu$ L) were added to each incubation sample. Mixtures were then incubated with trypsin (Roche Diagnostics, Indianapolis, IN) in a 1:25 (w/w) ratio overnight at room temperature. After proteolysis, the pH was adjusted to 5 by addition of 0.1% TFA followed by addition of ACN (5% final volume). Digested sample mixtures were immediately analyzed by LC-MS/MS. An Accela 1250 HPLC system coupled to an HTS PAL autosampler (LEAP Technologies, Carrboro, NC)

interfaced with an LTQ-Orbitrap Velos mass spectrometer (Thermo Fisher Scientific, Bremen, Germany) was used for peptide analysis. Peptide samples were injected onto a Phenomenex Jupiter C18 column (3  $\mu$ m, 2.1 x 150 mm; Torrance, CA). A flow rate of 0.2 mL/min, with a portion of the column elute (20%) diverted to the mass spectrometer. Mobile phase consisted of 0.05% formic acid in H<sub>2</sub>O (A) and 0.05% formic acid in ACN (B). Initial conditions were 98% A, with a linear gradient: 2% B for 2 min, 2–95% B over 35 min, and 95% B for 5 min. Ions were detected in positive mode; precursor masses were acquired in the FT-Orbitrap, while the top five most intense multiply charged ions in each MS spectrum were selected for fragmentation in the linear ion trap. Fragment ion spectra acquired from collision-induced dissociation (CID) were produced using 35% collision energy and a 1.0 Da isolation window. The resulting data were searched via SEQUEST embedded in Proteome Discoverer 1.2 (Thermo Scientific, San Jose, CA). The following SEQUEST parameters were modified to include exact masses associated with diquinone methide and o-quinone adducts to cysteine, lysine, glutamic acid, aspartic acid and tyrosine amino acids. A putative peptide adduct was sequenced utilizing the MS<sup>2</sup> data set, followed by additional MS<sup>3</sup> characterization to characterize the site of adduct formation.

*Structural Characterization and In Silico Modeling of CYP enzymes.* The PDB files used for modeling were 2HI4.pdb for CYP1A2, 1PQ2.pdb for CYP2C8, 1R9O.pdb for CYP2C9, 2F9Q.pdb for CYP2D6 and 1TQN.pdb for CYP3A4. For CYP2C19 a homology model was generated based upon the crystal structure of CYP2C9 (1RO9.pdb). For CYP3A5 a homology model was generated based upon the crystal structure of CYP3A4 (1TQN.pdb). Protein preparation script embedded in Maestro (Schrodinger, Portland, OR) was used to prepare the CYP structures prior to use in CAVER. Briefly, each pdb was imported and automatically corrected for missing hydrogens. All co-crystallized water molecules were removed and the iron formal charge defined at +3. Protonation states for histidine residues and heavy atoms in

arginine, glutamine and histamine side chains are also automatically assigned. The protein hydrogen bond network is also optimized prior to a final restrained minimization, which allows the hydrogen atoms to freely minimize within the protein. Prepared CYP structures were then explored using Caver as described (Petrek et al., 2006). In brief, the active site was defined by an active site water axial to the heme ligand. The default number of channels was explored with 4 angstroms of nearest neighbor. Protein cavities and tunnels were identified by analyses of a series of MD trajectory files with the Caver and visualized with PyMOL (Schrodinger, Portland, OR).

## Results

*Raloxifene metabolism and glutathione conjugate formation by CYP enzymes.* Figure 1 depicts the metabolic scheme for the CYP-mediated metabolism of raloxifene in vitro. All eight CYP isoforms tested exhibited different amounts of raloxifene oxidation. CYP2C19 showed the largest extent of raloxifene hydroxylation (Figure 2). In contrast, no evidence of CYP2E1 metabolite formation from raloxifene was observed. Metabolism experiments conducted in the presence of GSH determined the relative percent of reactive metabolite formation. CYP3A5 yielded the most GSH-related adducts when compared to the other CYP enzymes (Figure 2, Supplemental Figure 1). Differences in regioselectivity of glutathione adduct formation were also observed. For example, only CYP1A2, CYP3A4 and CYP3A5 demonstrated the potential to form adducts designated GSH1 and GSH2. GSH1 and GSH2 adduct are derived from the o-quinone ((Pearson et al., 2007), Figure 1). In contrast, all CYP enzymes examined formed GSH adducts from the precursor, diquinone methide, except for CYP2E1, where no GSH adducts were observed consistent with lack of raloxifene metabolism.

*Raloxifene-mediated CYP Inhibition.* Raloxifene demonstrated potential to inhibit each of the eight CYP enzymes, except CYP2E1. The inhibition ranged from 0.39 to 4.21  $\mu\text{M}$ . For CYP1A2, inhibition could not be readily determined based upon inability for fits to converge on the data (Table 1). Based upon the metabolism and inhibition across CYP isoforms, the potential for raloxifene mediated time-dependant inhibition (TDI) was assessed. An  $IC_{50}$  shift experiment was used to identify potential for TDI (Table 1). CYP2C8 and CYP3A4 showed a shift in potency from control samples greater than 2-fold. Based on the  $IC_{50}$  shift results, a full kinetic profile for TDI of CYP2C8 and CYP3A4 was performed. The  $K_i$  and  $k_{inact}$  for CYP2C8 was 0.26  $\mu\text{M}$  and 0.10  $\text{min}^{-1}$ , respectively. For CYP3A4, the  $K_i$  and  $k_{inact}$  were 0.81  $\mu\text{M}$  and 0.20  $\text{min}^{-1}$ , respectively (Table 1) and were similar to previous results (Chen et al., 2002).

*Identification of mechanism for raloxifene-mediated TDI of CYP2C8.* Raloxifene-mediated TDI in CYP2C8 was predicted to occur via apo-adduct formation based on quantitative recovery of heme and CO (data not shown). These results precluded heme adduct formation and metabolic-intermediate complex as mechanisms for CYP2C8 inactivation. Proteolysis of CYP2C8 following incubation with raloxifene and NADPH (n=4) yielded peptides covering 85-94% of the protein sequence, including a putative  $[M+3H]^{3+}$  peptide adduct at  $m/z$  724.0281 Da, corresponding to  $[M+H]^+ = 2170.0699$  Da. MS<sup>2</sup> experiments with  $m/z$  724.0281 serving as the precursor ion revealed doubly charged b and y ions (Figure 3) highlighted in blue and red, respectively. The y ion series with seven of the fourteen ions identified provided sufficient sequence coverage to identify the modified peptide as <sup>222</sup>LIDcFPGTHNKVLKN<sup>236</sup>, specifically y<sub>12</sub> is crucial in the identification of Cys225 as the adducted amino acid by bioactivation of raloxifene to the diquinone methide species, with a change in  $m/z$  of 471.1504. In addition, the theoretical molecular weight of the adducted peptide was consistent with the experimentally derived molecular weight ( $[M+H]^+ = 2170.0699$ ), differing by 9.1 ppm. The b ion series exhibited similar results with six ions identified including b<sub>4</sub>, consistent with Cys225 reacting with the diquinone methide species of raloxifene. The reaction of an active cysteine with the diquinone methide species of raloxifene is similar to the previous report of raloxifene adduct Cys239 of CYP3A4 (Baer et al., 2007). Subsequent MS<sup>3</sup> analysis conducted utilizing  $m/z$  724.0281 to 914.92 (y<sub>12</sub>) as precursors, generated product ions consistent with the adducted peptide (Supplemental Figure 2). Search algorithms were employed using raloxifene o-quinone mass for as a potential contributing inactivating species but no adducts were observed.

*Structural characterization of active site cysteine.* The program CAVER has been used to find the most accessible path from the active site to the surface of a protein (Petrek et al., 2006). Mapping of each CYP enzyme with CAVER revealed a conserved access channel for distal to the heme moving from the I-helix toward the end of the G and G' helices (Figure 4 ). Despite

this conserved channel, there were unique channels found for several of the CYPs. For example, primary access channel defined for CYP1A2 (2HI4.pdb) exits parallel to the I-Helix, between the G-Helix and I-Helix toward the K'  $\alpha$ -helix such that it runs parallel to the I-Helix (green channel, Figure 4A). A second egress channel begins to follow this trajectory but breaks toward the B'-Helix (orange channel, Figure 4A). In contrast, the cysteine residues with the closest proximity to the active site in CYP1A2 are located parallel to the heme adjacent to one another on the opposite side of the protein in the  $\beta$ 2 sheet region, Cys405 and Cys406. For CYP2C8, there are two cysteine (Cys216 and Cys225) residues distal to the heme. Upon overlay of CYP2C8 and CYP3A4 the placement of the Cys216 and Cys225 are in close proximity to the Cys239 for the respective enzymes (Figure 5). From the Caver results a unique access channel in CYP2C8 identified between B'-helix and G'-helix (green channel, Figure 4B). In contrast, the divergent channel in CYP3A4 was found to exit between the F'-helix and G'-helix (blue channel, Figure 4F). Based on the caver results and known substrate recognition sites, each CYP enzyme was positioned with the I-helix parallel to the z-axis and divided into four quadrants (Figure 4). All cysteine residues were identified in each of the quadrants (Table 2).

## Discussion

Mammalian CYP enzymes have a conserved globular tertiary structure (Johnson and Stout, 2005). At the core of CYP enzymes is a porphyrin heme, locked in place by electrostatic interactions with a number of conserved arginine residues and a ring of hydrophobic amino acids that sandwich the heme against the rigid, conserved I-Helix (Wester et al., 2004; Yano et al., 2004; Sansen et al., 2007; Halpert, 2011; Shah et al., 2011). Positioning the I-helix of each CYP parallel to the z-axis, each isoforms was divided into four quadrants to explore the location of cysteine residues (Figure 4A). In this view, the potential substrate and metabolite recognition sites are almost exclusively positioned in quadrant 1 (Q1) across the different mammalian CYPs. Therefore, the ability of a CYP enzyme to quench reactive metabolites is directed by the presence and accessibility of nucleophiles that can contact reactive metabolites in Q1. Reactive metabolites formed in CYP enzymes without matched nucleophiles could lead to uncontrolled reactive metabolite formation resulting in an increased exposure to reactive metabolites and potential for toxicity. Given the defined oxidative metabolic pathway and the previous characterization of glutathione adducts, raloxifene-mediated CYP bioactivation and inactivation was explored across eight CYP enzymes.

Raloxifene is an effective therapeutic in the treatment of breast cancer (Ko and Jordan, 2011). In vivo, the exposure and elimination of raloxifene is governed by gut glucuronidation (Kemp et al., 2002). However, in vitro raloxifene is subject to CYP3A metabolism resulting in the formation of multiple reactive metabolites, including a diquinone methide and o-quinone (Chen et al., 2002; Yu et al., 2004). The formation of the diquinone methide introduces an electrophilic structure capable of reacting at multiple sites over 12 angstroms, due to the extensive conjugation of the molecular structure (Figure 1). The diquinone methide reacts with soft nucleophiles such as glutathione and N-acetyl cysteine (Chen et al., 2002) but does not appear to react readily with more charge localized nucleophilic residues like lysine (data not shown). Additional reactivity of the diquinone methide has been shown toward acetic and

propionic acid suggesting potential for the diquinone methide to react with aspartic or glutamic acid under non physiological conditions (Moore et al., 2010). However, removal of Cys239 abolished TDI in CYP3A4 suggesting ester formation with diquinone methide is too unstable to lead to TDI. In addition, no isolable aspartic or glutamic acid raloxifene adducts were observed herein, albeit the transient nature of this complex could preclude isolation of the unstable peptide adduct. Based on the ability of raloxifene diquinone methide to readily react with cysteine, it serves as an excellent probe to explore the potential of CYP enzyme architecture for accessible cysteine residues.

Raloxifene incubations with all eight CYPs led to the formation of the diquinone methide except for CYP2E1 (Figure 2). In contrast, incubations setup to evaluate inactivation kinetics showed only CYP2C8 and CYP3A4 are susceptible to TDI (Table 1). An overlay of CYP2C8 and CYP3A4 structures revealed the presence of cysteine residues in Q1 for 2C8 similar to 3A4 (Figure 5). For CYP2C8, two cysteine residues were identified in Q1. Cys225 resides in helix F' and serves as the upper boundary to the CYP2C8 active site. Helix F' is also responsible for interactions with substrates in the active site (Schoch et al., 2008). The second cysteine, Cys216 resides at the start of helix G, also having the potential to interact with substrates and metabolites. In comparison, in CYP3A4 a single cysteine (Cys239) resides in the flexible loop preceding helix G.

Inactivation of CYP3A4 by raloxifene occurs through apo-adduct formation with Cys239 as previously demonstrated in reconstituted CYP3A4 enzyme (Baer et al., 2007). Confirmation of Cys239 adduction by raloxifene from CYP3A4 Supersomes<sup>TM</sup> is unique compared to previous efforts to identify CYP adducts which used purified, reconstituted enzyme (Lightning et al., 2000; Bateman et al., 2004; Wen et al., 2005; Yukinaga et al., 2007). A challenge with the reconstitution of recombinant CYPs is the complete incorporation of enzyme into the lipid membrane whereby any CYP left unincorporated into the lipid could trap reactive metabolites akin to an exogenously added nucleophile. Corroboration of the previously generated

recombinant data with CYP3A4 Supersomes™ confirms that Cys239 is the prominent residue involved in CYP3A4 inactivation. Therefore, the use of membrane prepared recombinant CYP enzymes should reduce the potential for falsely identified adducts while simultaneously increasing the speed and accuracy of adduct characterization.

The mechanism(s) behind raloxifene-mediated CYP2C8 inactivation did not occur through heme adduction or metabolic-intermediate complex formation (data not shown). Furthermore, given the structural alert and known propensity of raloxifene to form the diquinone methide, an apo-adduct(s) with CYP2C8 was hypothesized. A single raloxifene adduct was identified at Cys225 with a mass consistent of addition of the diquinone methide metabolite. Not surprisingly, Cys225 from CYP2C8 and Cys239 from CYP3A4 approximate the same spatial arrangement upon overlay of the two structures (Figure 5). Cys216 in CYP2C8 is in close proximity to Cys225. A noteworthy finding is that both CYP2C9 and CYP2C19 also possess Cys216 similar to that found in CYP2C8. Upon overlay of the all of the CYP2C structures, Cys216 resides in a similar space for each enzyme. The lack of adduct formation at Cys216 with raloxifene in CYP2C8 is also consistent with the lack of TDI observed in both CYP2C9 and CYP2C19.

The surrounding protein environment also greatly impacts nucleophilicity of the cysteine thiols (Ferrer-Sueta et al., 2011). In addition, many protein surface thiols are often targets for oxidation (Requejo et al., 2010). Based upon the uncoupling of CYP catalytic cycle and ability to generate hydrogen peroxide, there is a potential for cysteines near active site to undergo oxidation to sulfenic acid. Sulfenic acid is highly reactive and capable of undergoing nucleophilic attack or additional oxidations ultimately to stable sulfonic acid derivative (Romero et al., 1992; Liu et al., 1996; Claiborne et al., 2001). Analysis of peptide digests for oxidized cysteines revealed that all of the CYP2C8 digests possessed a peptide containing oxidized Cys216 (SO<sub>3</sub>H). Therefore, the oxidation of Cys216 could easily compromise reactivity toward various electrophiles.

In addition, the absence of a Cys216 raloxifene adduct could be a result of specific egress channel of the diquinone methide that traverses proximal to Cys225. Utilizing Caver, access channels in CYP2C8 were modeled in an attempt to gain further insight to the regioselectivity demonstrated by raloxifene diquinone methide. Three primary channels were observed for CYP2C8. The largest channel in CYP2C8 overlaps with that determined in CYP3A4. In addition, the second most prominent channel traverses a similar path between CYP2C8 and CYP3A4. The second channel passes in close proximity to Cys225 and Cys239 in CYP2C8 and CYP3A4, respectively. No access channels were shown to pass directly by Cys216 consistent with the unmodified peptide observed in the digest. The combined data support the notion that CYP2C8 TDI is mediated through the raloxifene diquinone methide predominantly, if not exclusively, by Cys225.

The lack of raloxifene mediated inactivation of CYP1A2, CYP2D6 and CYP3A5 are consistent with the lack of cysteine residues present in Q1. However, numerous examples of TDI have been documented with the aforementioned enzymes. Many of the examples cause TDI through MI complex formation and are not applicable to this discussion (VandenBrink and Isoherranen, 2010). However, examples where TDI is likely to occur by apo-adduct formation exist. For example, CYP2D6 inactivation was observed with EMTPP as an apo-adduct (Hutzler et al., 2004). The exact site and residue of adduct formation was never pursued. CYP1A2 mediated metabolism of zileuton also leads to TDI for which the mechanism is hypothesized to occur through apo-adduct formation (Lu et al., 2003). There are two interesting concepts conserved across these TDI examples: 1) glutathione adducts for the drugs have been identified implicating the potential for apo-protein formation and 2) there are a lack of cysteine residues in Q1. A potential explanation for the disconnect between the observed inactivation and the absence of Q1 cysteines would be the potential for novel egress channels beyond Q1. For CYP1A2, there are two cysteine residues that reside in close proximity to the active site, Cys405 and Cys406. However, the CYP1A2 egress channels produced in Caver do not

converge upon residues Cys405 or Cys406 or any other cysteine residues within the enzyme. Conversely, the reactive metabolites may have sufficient electrophilic properties to react with other less commonly described nucleophiles; additional research is warranted to link these reactive metabolites to CYP inactivation. Moreover, based upon these structures and predicted access channels other drugs prone to bioactivation and reactivity toward soft electrophiles may also be capable of escaping the active site without enzyme inactivation. Reactive metabolites with similar reactivity suggest CYP clearance pathways could influence exposure to reactive metabolites and exacerbate drug-induced liver injury. Exploration of this with more relevant drugs, for example, drugs that are cleared in vivo by different CYPs that concurrently show potential for hepatotoxicity will ultimately enable further testing of this hypothesis.

In conclusion, all of the CYP enzymes examined (except CYP2E1) formed the diquinone methide thus providing a probe of each active site for solvent accessible cysteines capable of enzyme inactivation. Similar to CYP3A4, an active site Cys residue in CYP2C8 is alkylated upon raloxifene bioactivation to the diquinone methide to inactivate the enzyme. The inability for inactivation by the diquinone methide with CYP 1A2, 2D6 and 3A5 are consistent with the crystal structure data wherein no cysteines are present in Q1. Additional support from the Caver derived access channels clearly demonstrates the primary metabolite exit channels are void of cysteine residues capable of trapping the raloxifene diquinone methide. The inability to inactivate CYP2C9 and CYP2C19 could be due to oxidation of Cys216 similar to reports here with CYP2C8. Finally, the combined data presented suggests the extent of reactive metabolite formation by a CYP enzyme does not correlate to CYP inactivation. Multiple factors, including active site architecture, exit channels and chemical structure of the reactive metabolite all may contribute to the ability to form apo-adducts with a CYP enzyme.

## Authorship Contributions

Participated in research design: VandenBrink, Davis, Pearson, Foti, Wienkers and Rock

Conducted experiments: VandenBrink, Davis, Pearson, Foti and Rock

Contributed new reagents or analytic tools: none

Performed data analysis: VandenBrink, Davis, Pearson, Foti and Rock

Wrote or contributed to the writing of the manuscript: VandenBrink and Rock

## References

- Baer BR, Wienkers LC, and Rock DA (2007) Time-dependent inactivation of P450 3A4 by raloxifene: identification of Cys239 as the site of apoprotein alkylation. *Chem Res Toxicol* **20**:954-964.
- Baillie TA, Pearson PG, Rashed MS, and Howald WN (1989) The use of mass spectrometry in the study of chemically-reactive drug metabolites. Application of MS/MS and LC/MS to the analysis of glutathione- and related S-linked conjugates of N-methylformamide. *J Pharm Biomed Anal* **7**:1351-1360.
- Bateman KP, Baker J, Wilke M, Lee J, Leriche T, Seto C, Day S, Chauret N, Ouellet M, and Nicoll-Griffith DA (2004) Detection of covalent adducts to cytochrome P450 3A4 using liquid chromatography mass spectrometry. *Chem Res Toxicol* **17**:1356-1361.
- Chan WK, Sui Z, and Ortiz de Montellano PR (1993) Determinants of protein modification versus heme alkylation: inactivation of cytochrome P450 1A1 by 1-ethynylpyrene and phenylacetylene. *Chem Res Toxicol* **6**:38-45.
- Chen Q, Ngui JS, Doss GA, Wang RW, Cai X, DiNinno FP, Blizzard TA, Hammond ML, Stearns RA, Evans DC, Baillie TA, and Tang W (2002) Cytochrome P450 3A4-mediated bioactivation of raloxifene: irreversible enzyme inhibition and thiol adduct formation. *Chem Res Toxicol* **15**:907-914.
- Claiborne A, Mallett TC, Yeh JJ, Luba J, and Parsonage D (2001) Structural, redox, and mechanistic parameters for cysteine-sulfenic acid function in catalysis and regulation. *Adv Protein Chem* **58**:215-276.
- Dahlin DC, Miwa GT, Lu AY, and Nelson SD (1984) N-acetyl-p-benzoquinone imine: a cytochrome P-450-mediated oxidation product of acetaminophen. *Proc Natl Acad Sci U S A* **81**:1327-1331.
- Dickmann LJ, Vandenbrink BM, and Lin YS (2012) In Vitro Hepatotoxicity and Cytochrome P450 Induction and Inhibition Characteristics of Carnosic Acid, a Dietary Supplement with Antiadipogenic Properties. *Drug Metab Dispos*.
- Dieckhaus CM, Fernandez-Metzler CL, King R, Krolikowski PH, and Baillie TA (2005) Negative ion tandem mass spectrometry for the detection of glutathione conjugates. *Chem Res Toxicol* **18**:630-638.
- Dong D and Wu B (2012) Substrate selectivity of drug-metabolizing cytochrome P450s predicted from crystal structures and in silico modeling. *Drug Metab Rev* **44**:1-17.
- Ferrer-Sueta G, Manta B, Botti H, Radi R, Trujillo M, and Denicola A (2011) Factors affecting protein thiol reactivity and specificity in peroxide reduction. *Chem Res Toxicol* **24**:434-450.
- Guengerich FP (2001) Common and Uncommon Cytochrome P450 Reactions Related to Metabolism and Chemical Toxicity. **14**:611-650.
- Halpert JR (2011) Structure and function of cytochromes P450 2B: from mechanism-based inactivators to X-ray crystal structures and back. *Drug Metab Dispos* **39**:1113-1121.
- Hanson KL, VandenBrink BM, Babu KN, Allen KE, Nelson WL, and Kunze KL (2010) Sequential metabolism of secondary alkyl amines to metabolic-intermediate complexes: opposing roles for the secondary hydroxylamine and primary amine metabolites of desipramine, (s)-fluoxetine, and N-desmethyldiltiazem. *Drug Metab Dispos* **38**:963-972.

- Henne KR, Tran TB, Vandenbrink BM, Rock DA, Aidasani DK, Subramanian R, Mason AK, Stresser DM, Teffera Y, Wong SG, Johnson MG, Chen X, Tonn GR, and Wong BK (2012) Sequential Metabolism of AMG 487, a Novel CXCR3 Antagonist, Results in Formation of Quinone Reactive Metabolites that Covalently Modify CYP3A4 Cys239 and Cause Time-Dependent Inhibition of the Enzyme. *Drug Metab Dispos*.
- Hutzler JM, Steenwyk RC, Smith EB, Walker GS, and Wienkers LC (2004) Mechanism-based inactivation of cytochrome P450 2D6 by 1-[(2-ethyl-4-methyl-1H-imidazol-5-yl)methyl]-4-[4-(trifluoromethyl)-2-pyridinyl]piperazine: kinetic characterization and evidence for apoprotein adduction. *Chem Res Toxicol* **17**:174-184.
- Johnson EF and Stout CD (2005) Structural diversity of human xenobiotic-metabolizing cytochrome P450 monooxygenases. *Biochem Biophys Res Commun* **338**:331-336.
- Kalgutkar AS and Didiuk MT (2009) Structural alerts, reactive metabolites, and protein covalent binding: how reliable are these attributes as predictors of drug toxicity? *Chem Biodivers* **6**:2115-2137.
- Kalgutkar AS, Obach RS, and Maurer TS (2007) Mechanism-based inactivation of cytochrome P450 enzymes: chemical mechanisms, structure-activity relationships and relationship to clinical drug-drug interactions and idiosyncratic adverse drug reactions. *Curr Drug Metab* **8**:407-447.
- Kang P, Liao M, Wester MR, Leeder JS, Pearce RE, and Correia MA (2008) CYP3A4-Mediated carbamazepine (CBZ) metabolism: formation of a covalent CBZ-CYP3A4 adduct and alteration of the enzyme kinetic profile. *Drug Metab Dispos* **36**:490-499.
- Kemp DC, Fan PW, and Stevens JC (2002) Characterization of raloxifene glucuronidation in vitro: contribution of intestinal metabolism to presystemic clearance. *Drug Metab Dispos* **30**:694-700.
- Ko SS and Jordan VC (2011) Treatment of osteoporosis and reduction in risk of invasive breast cancer in postmenopausal women with raloxifene. *Expert Opin Pharmacother* **12**:657-674.
- Kunze KL and Trager WF (1993) Isoform-selective mechanism-based inhibition of human cytochrome P450 1A2 by furafylline. *Chem Res Toxicol* **6**:649-656.
- Leung L, Kalgutkar AS, and Obach RS (2012) Metabolic activation in drug-induced liver injury. *Drug Metab Rev* **44**:18-33.
- Lewis DF and Lake BG (1996) Molecular modelling of CYP1A subfamily members based on an alignment with CYP102: rationalization of CYP1A substrate specificity in terms of active site amino acid residues. *Xenobiotica* **26**:723-753.
- Lightning LK, Jones JP, Friedberg T, Pritchard MP, Shou M, Rushmore TH, and Trager WF (2000) Mechanism-based inactivation of cytochrome P450 3A4 by L-754,394. *Biochemistry* **39**:4276-4287.
- Lin HL, Kenaan C, and Hollenberg PF (2012) Identification of the Residue in Human CYP3A4 That Is Covalently Modified by Bergamottin and the Reactive Intermediate That Contributes to the Grapefruit Juice Effect. *Drug Metab Dispos* **40**:998-1006.
- Liu H, Lightfoot R, and Stevens JL (1996) Activation of heat shock factor by alkylating agents is triggered by glutathione depletion and oxidation of protein thiols. *J Biol Chem* **271**:4805-4812.
- Lu P, Schrag ML, Slaughter DE, Raab CE, Shou M, and Rodrigues AD (2003) Mechanism-based inhibition of human liver microsomal cytochrome P450 1A2 by zileuton, a 5-lipoxygenase inhibitor. *Drug Metab Dispos* **31**:1352-1360.

- Mitchell JR, Jollow DJ, Potter WZ, Davis DC, Gillette JR, and Brodie BB (1973) Acetaminophen-induced hepatic necrosis. I. Role of drug metabolism. *J Pharmacol Exp Ther* **187**:185-194.
- Moore CD, Reilly CA, and Yost GS (2010) CYP3A4-Mediated oxygenation versus dehydrogenation of raloxifene. *Biochemistry* **49**:4466-4475.
- Nelson SD (1982) Metabolic activation and drug toxicity. *J Med Chem* **25**:753-765.
- Pearson JT, Wahlstrom JL, Dickmann LJ, Kumar S, Halpert JR, Wienkers LC, Foti RS, and Rock DA (2007) Differential time-dependent inactivation of P450 3A4 and P450 3A5 by raloxifene: a key role for C239 in quenching reactive intermediates. *Chem Res Toxicol* **20**:1778-1786.
- Petrek M, Otyepka M, Banas P, Kosinova P, Koca J, and Damborsky J (2006) CAVER: a new tool to explore routes from protein clefts, pockets and cavities. *BMC Bioinformatics* **7**:316.
- Requejo R, Chouchani ET, Hurd TR, Menger KE, Hampton MB, and Murphy MP (2010) Measuring mitochondrial protein thiol redox state. *Methods Enzymol* **474**:123-147.
- Romero FJ, Ordonez I, Arduini A, and Cadenas E (1992) The reactivity of thiols and disulfides with different redox states of myoglobin. Redox and addition reactions and formation of thiyl radical intermediates. *J Biol Chem* **267**:1680-1688.
- Sansen S, Yano JK, Reynald RL, Schoch GA, Griffin KJ, Stout CD, and Johnson EF (2007) Adaptations for the oxidation of polycyclic aromatic hydrocarbons exhibited by the structure of human P450 1A2. *J Biol Chem* **282**:14348-14355.
- Schoch GA, Yano JK, Sansen S, Dansette PM, Stout CD, and Johnson EF (2008) Determinants of cytochrome P450 2C8 substrate binding: structures of complexes with montelukast, troglitazone, felodipine, and 9-cis-retinoic acid. *J Biol Chem* **283**:17227-17237.
- Shah MB, Pascual J, Zhang Q, Stout CD, and Halpert JR (2011) Structures of cytochrome P450 2B6 bound to 4-benzylpyridine and 4-(4-nitrobenzyl)pyridine: insight into inhibitor binding and rearrangement of active site side chains. *Mol Pharmacol* **80**:1047-1055.
- Silverman RB (1988) *Mechanism-based Enzyme Inactivation: Chemistry and Enzymology*. CRC Press.
- Stepan AF, Walker DP, Bauman J, Price DA, Baillie TA, Kalgutkar AS, and Aleo MD (2011) Structural alert/reactive metabolite concept as applied in medicinal chemistry to mitigate the risk of idiosyncratic drug toxicity: a perspective based on the critical examination of trends in the top 200 drugs marketed in the United States. *Chem Res Toxicol* **24**:1345-1410.
- VandenBrink BM and Isoherranen N (2010) The role of metabolites in predicting drug-drug interactions: focus on irreversible cytochrome P450 inhibition. *Curr Opin Drug Discov Devel* **13**:66-77.
- Wen B, Doneanu CE, Gartner CA, Roberts AG, Atkins WM, and Nelson SD (2005) Fluorescent photoaffinity labeling of cytochrome P450 3A4 by lapachenole: identification of modification sites by mass spectrometry. *Biochemistry* **44**:1833-1845.
- Wester MR, Yano JK, Schoch GA, Yang C, Griffin KJ, Stout CD, and Johnson EF (2004) The structure of human cytochrome P450 2C9 complexed with flurbiprofen at 2.0-A resolution. *J Biol Chem* **279**:35630-35637.
- Wienkers LC and Heath TG (2005) Predicting in vivo drug interactions from in vitro drug discovery data. *Nat Rev Drug Discov* **4**:825-833.

- Yano JK, Wester MR, Schoch GA, Griffin KJ, Stout CD, and Johnson EF (2004) The structure of human microsomal cytochrome P450 3A4 determined by X-ray crystallography to 2.05-Å resolution. *J Biol Chem* **279**:38091-38094.
- Yu L, Liu H, Li W, Zhang F, Luckie C, van Breemen RB, Thatcher GR, and Bolton JL (2004) Oxidation of raloxifene to quinoids: potential toxic pathways via a diquinone methide and o-quinones. *Chem Res Toxicol* **17**:879-888.
- Yukinaga H, Takami T, Shioyama SH, Tozuka Z, Masumoto H, Okazaki O, and Sudo K (2007) Identification of cytochrome P450 3A4 modification site with reactive metabolite using linear ion trap-Fourier transform mass spectrometry. *Chem Res Toxicol* **20**:1373-1378.

## Legends for Figures

Figure 1. Structures of raloxifene and major P450 metabolite and reactive intermediates inferred from GSH adducts A) 3'-hydroxy raloxifene, B) diquinone methide, C) 6,7-o-quinone.

Figure 2. Raloxifene metabolite formation across CYP enzymes. GSH1 and GSH2 are glutathione products from the 6, 7- o-quinone, pathway C, Figure 1 (A), GSH 3,4 and 5 were derived from the diquinone methide, pathway B, Figure1 (B) and oxidized 3' hydroxy raloxifene, pathway A, Figure 1 (C). Percentages of metabolites formed are represented in triplicate. \*( increased by 5X)

Figure 3. Mass spectra of the CYP2C8 raloxifene-adducted peptide, 222-LIDcFPGTHNKVLKN-236. Spectrum acquired at 24.1 min with parent  $[M+3H]^{3+} = m/z$  724.0281 corresponding to a mass error of 9.1 ppm. Blue ions (y ions) and red ions (b ions) masses are listed in the table to the right of the ions labeled on the MS/MS spectra.

Figure 4. Active site access channels found by identified with Caver in cytochrome: (A) CYP1A2, (B) CYP2C8, (C) CYP2C9, (D) CYP2C19, (E) CYP2D6, and (F) CYP3A4. The top three trajectories depicted as tubes showing the route followed by the center of mass of the substrate raloxifene. Each structure is divided into 4 quadrants using the I-Helix as the intersection point. Helices are labeled in corresponding red letters.

Figure 5: Structures of CYP2C8 (cyan) and CYP3A4 (dark blue) overlaid. The heme is depicted in purple, cysteine residue associated with CYP2C8 and CYP3A4 are in red and green, respectively. Raloxifene docked in the active site as a point of reference in yellow.

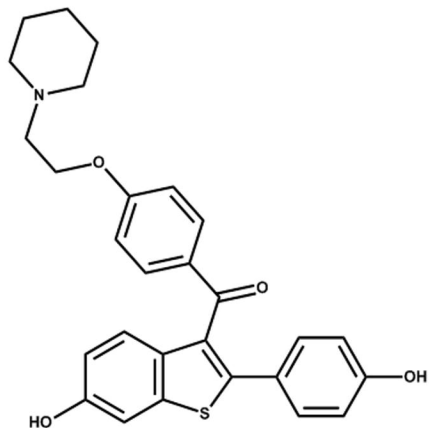
**Table 1. Raloxifene-mediated CYP inhibition kinetic constant, where NA, not available and NI, no inhibition**

<b>CYP</b>	<b>IC<sub>50</sub> (<math>\mu</math>M)</b>	<b>IC<sub>50</sub> Shift (<math>\mu</math>M)</b>	<b>K<sub>i</sub> (<math>\mu</math>M)</b>	<b>k<sub>inact</sub> (min<sup>-1</sup>)</b>	<b>Partition Ratio</b>
<b>1A2</b>	<b>NA</b>	<b>No</b>	<b>-</b>	<b>-</b>	<b>-</b>
<b>2C8</b>	<b>1.10</b>	<b>Yes</b>	<b>0.26</b>	<b>0.1</b>	<b>3.1</b>
<b>2C9</b>	<b>0.39</b>	<b>No</b>	<b>-</b>	<b>-</b>	<b>-</b>
<b>2C19</b>	<b>2.01</b>	<b>No</b>	<b>-</b>	<b>-</b>	<b>-</b>
<b>2D6</b>	<b>4.21</b>	<b>No</b>	<b>-</b>	<b>-</b>	<b>-</b>
<b>2E1</b>	<b>NI</b>	<b>No</b>	<b>-</b>	<b>-</b>	<b>-</b>
<b>3A4</b>	<b>0.78</b>	<b>Yes</b>	<b>0.81</b>	<b>0.2</b>	<b>1.9</b>
<b>3A5</b>	<b>2.85</b>	<b>No</b>	<b>-</b>	<b>-</b>	<b>-</b>

**Table 2. Location of cysteine residues in each quadrant across the CYP enzymes. A. Indicates residues in Q1 but with limited access to active sites: In CYP1A2, cysteine 405 is in  $\beta$ 2 sheet with thiol in contact with bulk solvent and pointed toward N-terminus. In CYP2D6, cysteine 57 is at the start of the helix-A which exterior to  $\beta$ 1 and  $\beta$ 2 leaving the thiol exposed to bulk solvent. B. Axial cysteine coordinating heme iron.**

CYP	1A2	2C8	2C9	2C19	2D6	3A4	3A5
Q1	405 406	216 225	216	216	57	58 64 98 239 377	64 98 377
Q2	204 504	151 164 172 175 179 486	151 164 172 175 179	151 164 172 175 179	159 161 191 493	468	467
Q3	458	435	372 435	372 435	443	442	441
Q4	159	266 338	266 336	266 338	NA	NA	NA

Figure 1



**Raloxifene**

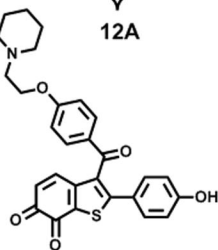
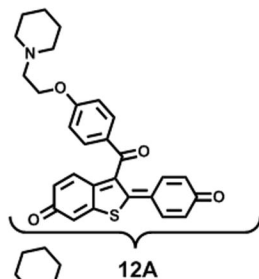
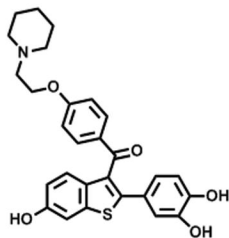
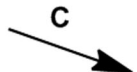
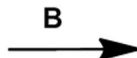


**Figure 2**

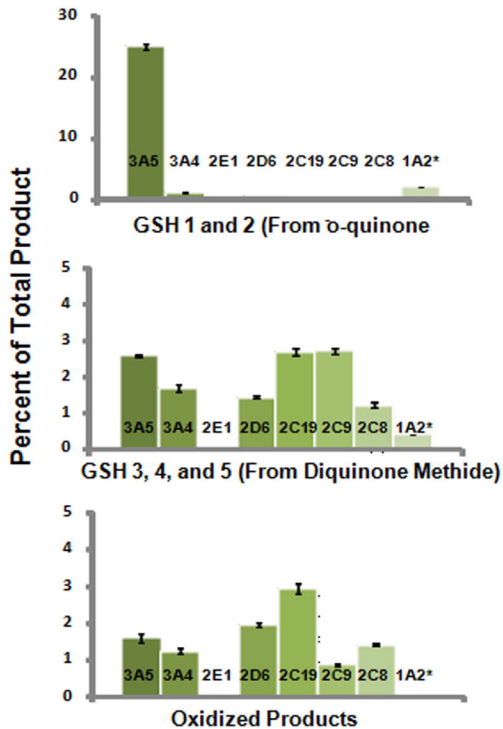


Figure 3.

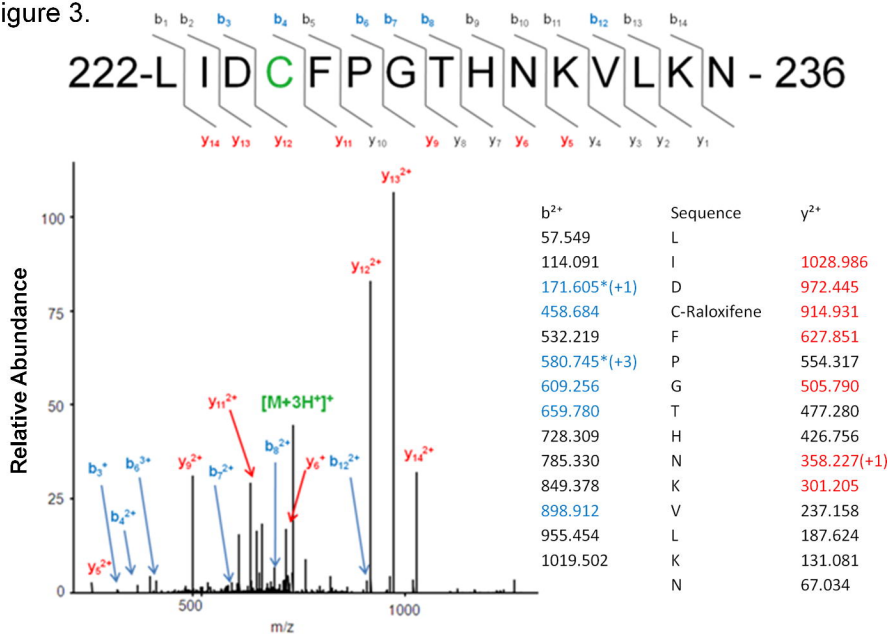


Figure 4.

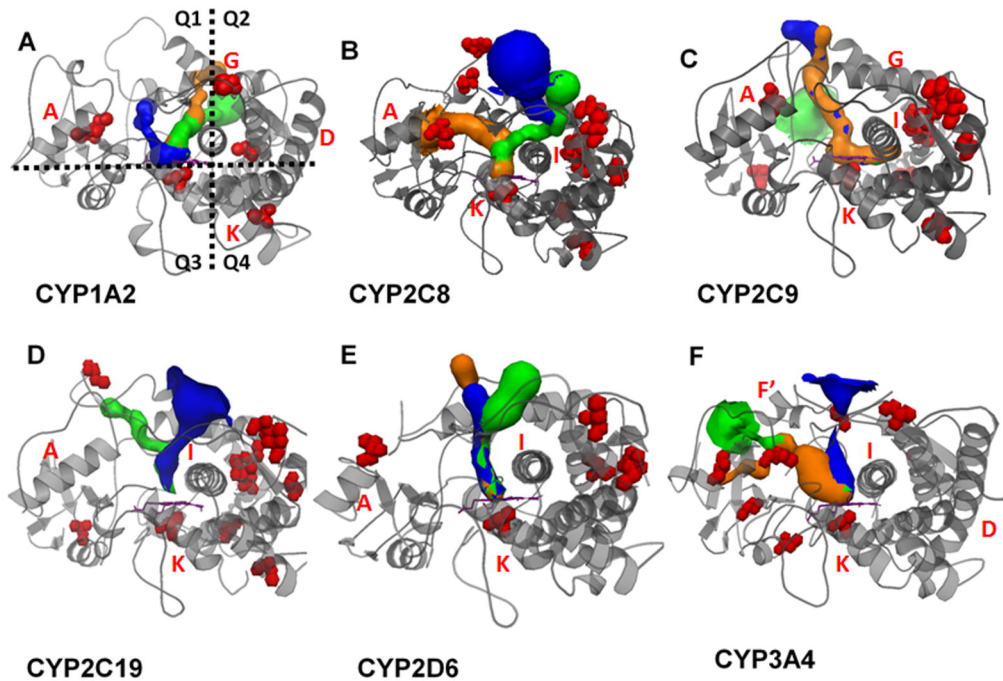


Figure 5

